J. Physiol. (1986), **371**, *pp.* 115–145
With 19 *text-figures*
Printed in Great Britain

ELECTRICAL PROPERTIES OF THE LIGHT-SENSITIVE CONDUCTANCE OF RODS OF THE SALAMANDER *AMBYSTOMA TIGRINUM*

BY D. A. BAYLOR AND B. J. NUNN*

From the Department of Neurobiology, Stanford University School of Medicine, Stanford, CA 94305, U.S.A.

(*Received 19 March 1985*)

SUMMARY

1. The light-sensitive conductance of isolated rods from the retina of the tiger salamander was studied using a voltage-clamp method. The membrane current of the outer segment was collected with a suction electrode while the internal voltage was measured and controlled with a pair of intracellular electrodes.

2. Saturating light blocked the outer segment current at all potentials, the residual conductance usually becoming less than 20 pS. This suggests that light-sensitive channels comprise the main ionic conductance in the surface membrane of the outer segment.

3. Current–voltage relations determined 10–40 ms after changing the voltage showed outward-going rectification, the outward current increasing e-fold for a depolarization of 11–14 mV.

4. The reversal potential of the light-sensitive current was estimated as 5 ± 4 mV. This is consistent with other evidence indicating that the channel is not exclusively permeable to Na.

5. Applying steady light, lowering external Ca, or changing the intracellular voltage to a new steady level scaled the light-sensitive current without altering the reversal potential or the form of the rectification. This suggests that all three manipulations change the number of channels in the conducting state without changing the ionic concentration gradients or the mechanism of permeation through an 'open' channel.

6. Hyperpolarizing voltage steps slowly increased the light-sensitive current and depolarizing steps reduced it. A gating variable Y expressing the fractional activation of the light-sensitive conductance in the steady state was derived from the ratio of the instantaneous and steady-state currents. Y declined at voltages positive to -100 mV and usually reached a minimum near 0 mV, with a secondary rise positive to 0 mV. Around the dark voltage Y changed e-fold in roughly 25 mV.

7. The voltage-dependent gating in (6). appeared to involve two delays similar in magnitude to those of the four principal delays in the rod's response to a dim flash. Steady background light shortened the time-scale of gating and flash responses to a similar degree.

* Present address: Physiological Laboratory, Downing Street, Cambridge CB2 3EG.

8. Clamping the voltage at the dark level had little effect on the photocurrent evoked by a flash. The small, delayed effect actually observed is explained by the slow voltage-dependent gating of the light-sensitive conductance.

9. Hyperpolarization had little effect on the kinetics of the response to a flash, but depolarization slowed the response, causing it to reach a larger, later peak. Depolarization also prolonged the blockage of the light-sensitive current after a saturating flash.

10. We conclude that the voltage at the surface membrane of the outer segment modulates the internal chemistry that controls the light-sensitive conductance. The voltage effects have some of the properties expected if they originate at the electrogenic Na–Ca exchange thought to be present in the surface membrane.

INTRODUCTION

Photoisomerization of rhodopsin in a vertebrate rod triggers a series of steps that culminate in the reduction of a steady inward current of Na ions at the membrane of the outer segment (Hagins, Penn & Yoshikami, 1970). The electrical properties of the light-sensitive conductance are not well understood. Information about the voltage dependence of the conductance may help to clarify the nature of the light-sensitive pores or carrier molecules.

In these experiments the light-sensitive current of an isolated rod was measured with a suction electrode while the internal potential was controlled with a double-electrode voltage clamp. The results confirm and extend previous observations from current-clamp experiments (Baylor, Matthews & Nunn, 1984), which revealed a slow voltage-dependent gating of the light-sensitive conductance as well as a very low outer segment conductance in saturating light. Related experiments on the light-sensitive conductance of isolated salamander rods have been made by Bader, MacLeish & Schwartz (1979) and MacLeish, Schwartz & Tachibana (1984).

METHODS

Animals and preparation

Larval tiger salamanders (*Ambystoma tigrinum*) were kept at 4 °C in a modified Holtfreter solution (Nace, 1974) containing aquarium vitamin drops and (in mM): NaCl, 30; KCl, 0·34; $CaCl_2$, 0·23; $NaHCO_3$, 1·2 and EDTA, 0·004. This solution was aerated, recirculated through charcoal filters and changed every two weeks. Other aspects of animal care, as well as the method of obtaining isolated dark-adapted rods by chopping the retina, are described in Baylor *et al.* (1984).

Electrodes

Suction electrodes and intracellular electrodes with a right angle bend were made as described in Baylor *et al.* (1984). The intracellular electrodes were filled with 0·5 M-K acetate (see Baylor *et al.* 1984) and a coating of silver paint applied to within 2 mm of the bend. After the paint dried, several coats of rubber cement insulation were applied. During painting and coating the tips of the electrodes were kept clean by immersion in flowing filtered water. Satisfactory intracellular electrodes were very gently tapered near the tip and had resistances of 500–1000 MΩ.

Changes in tip potential were measured in a sample of eleven intracellular electrodes immersed in Ringer solution or 0·1 M-KCl, which was used to simulate the intracellular solution. The arrangement was:

salamander Ringer: test solution	3 M-KCl agar: bridge	calomel half-cell: to earth	3 M-KCl agar: bridge	100 mM-KCl test solution

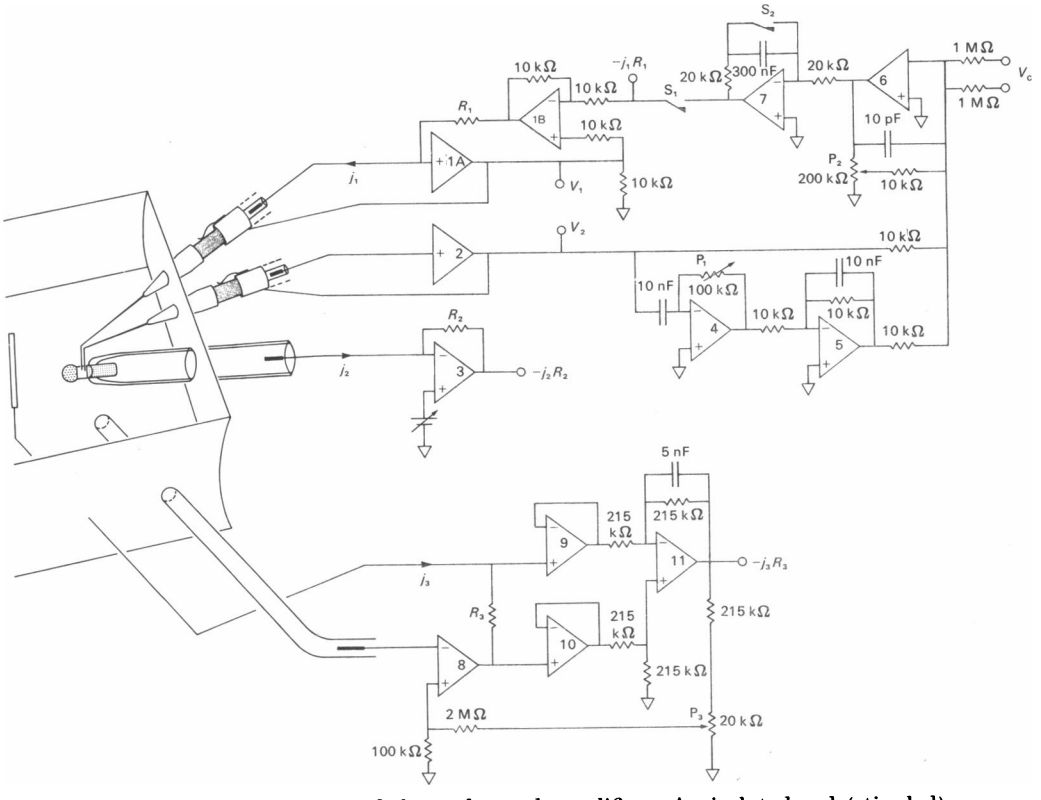

Fig. 1. Schematic diagram of electrodes and amplifiers. An isolated rod (stippled) was held in the suction electrode and impaled with intracellular electrodes for recording its internal voltage and passing current. Before voltage clamping, bright flash responses were observed at V_1 and V_2. Small constant current steps were injected through amplifier 1 and the changes in potential observed at V_2. For voltage clamping, switch S_1 was closed, S_2 opened and the slider of P_2 moved down to increase the feed-back gain. Final adjustment involved increasing P_1 and varying P_2 so that a square wave applied at V_c elicited a voltage change without damped oscillations. Voltage amplifiers 1 and 2 were Dagan model 8100 (WPI M701 in earlier experiments) and WPI model M707 respectively, connected to the micro-electrodes with Ag–AgCl junctions. Input connexions to current-measuring amplifier 3 and bath clamp amplifier 8 were via calomel half cells and salt bridges. The output of amplifier 8 was connected to the bath with a Pt wire. In the circuit diagram several buffer amplifiers, stopper resistors, voltage offset resistors and similar elements have been omitted. Resistor R_1 was 20 MΩ and the corresponding resistor (not shown) in amplifier 2 was 200 MΩ. Current-measuring resistors R_2 and R_3 were 100 MΩ and 500 MΩ, respectively. Voltage drops across R_1, R_2 and R_3 are proportional to currents j_1, j_2, and j_3. Amplifiers 3, 9, 10, 11 were Function Modules 380K; amplifier 8 Analog Devices 52K; 4 and 5 National Semiconductor LF356; 6 and 7 Signetics NE 5534.

The electrode was alternately dipped into the Ringer and KCl test solutions while recording its potential with respect to earth. The mean potential change observed on going from Ringer to KCl was +3·0 mV (range +1 to +5 mV). These measurements suggest that recorded membrane voltages may be about 3 mV positive to the true values. Voltages are given as recorded except where otherwise noted.

Electrical recording and voltage clamp

The electrodes and amplifiers are shown in Fig. 1. The membrane current, j_2, collected from the outer segment by the suction electrode, gave a voltage $-j_2R_2$ at the output of amplifier 3. The intracellular micro-electrodes were led to unity-gain voltage amplifiers 1 and 2. The electrode connected to amplifier 2 was used exclusively for measuring internal voltage. Amplifier 1 was used to record voltage from the second intracellular electrode while penetrating the cell, and for passing current into it using the voltage-to-current converter 1 B. The output of each voltage amplifier was

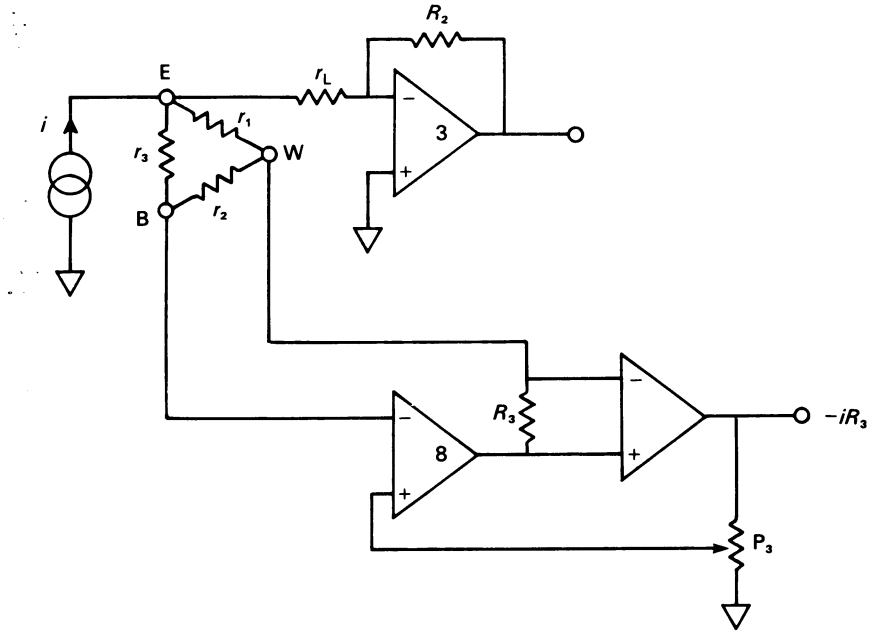

Fig. 2. Principle of operation of bath clamp compensation circuit. In this simplified diagram, amplifiers 3 and 8 and resistors R_2, R_3 and P_3 are as in Fig. 1. r_L is leakage resistance at mouth of suction electrode, r_1, r_2 and r_3 lumped solution resistances. W is the platinum current return wire in the bath, B the voltage-measuring port of the bath amplifier, and E the tip of the current-passing intracellular electrode. E assumed to be just outside the rod, as during adjustment of compensation potentiometer P_3.

connected to a metal shield around the electrode holder and to the silver paint on the electrode. This 'driven shield' arrangement reduced capacitive interaction between the electrodes and improved their frequency response. In some experiments the driven shield on the current-passing electrode was omitted. Before impalements the negative capacitance controls of amplifiers 1 and 2 were adjusted to increase the frequency response of the clamping circuit.

For voltage clamping switch S_1 was closed. Amplifier 1 B injected current j_1 into the rod to bring the membrane potential V_2 to a value set by the command potential V_c. Amplifier 7 had a very large low-frequency gain when switch S_2 was opened. Additional variable gain was selected at potentiometer P_2. The frequency response of the feed-back circuit was adjusted by potentiometer P_1 on amplifier 4, which added to the measured voltage a signal proportional to the rate of change of membrane potential. P_1 was adjusted by applying a voltage step at V_c and observing V_2. P_1 was increased so that V_2 showed a slightly underdamped rise to the final level.

The circuit at the bottom of Fig. 1 held the voltage at the tip of the suction electrode at ground potential during current injection, preventing inner segment current from entering the suction electrode through the small leakage space between the wall of the suction electrode and the cell

membrane. This arrangement allowed measurement of the outer segment current with minimal contamination from inner segment current. Without the compensation, leakage current added to the true outer segment current, j_2, and lowered the apparent membrane resistance of the outer segment in saturating light. The compensation circuit also allowed measurement of the membrane current, j_3, of the portion of the rod protruding from the suction electrode.

The principle of operation of the compensation circuit is shown in Fig. 2. A current i injected into the bath near the tip of the suction electrode (E) flowed to the bath return wire (W) and caused a voltage drop iR_3 in resistor R_3. This voltage was inverted and a small fraction k of it was selected at P_3 and applied to the non-inverting input of amplifier 8. This biased the voltage-sensing port (B) in the chamber by the same amount. The voltage divider in the solution 'levered' W further negative, allowing E to remain at ground voltage. For the circuit in Fig. 2 compensation is independent of i for a voltage fraction $k = r_1 r_3 / R_3(r_1 + r_2 + r_3)$. In an experiment P_3 was adjusted with the rod in the suction electrode but before penetration by the intracellular electrodes. With the tip of the current-injecting electrode just outside the cell large current pulses were passed and the slider of P_3 moved to eliminate the pulses of leakage current recorded by amplifier 3. The same setting of P_3 was assumed to be appropriate when the current-injection electrode was intracellular; this is not strictly so because the source geometry is different when current is delivered by the entire surface of the inner segment rather than from a point, as when the compensation was set. Resolution of currents j_2 and j_3 was limited by thermal noise in the leakage resistance at the tip of the suction electrode. Current j_3 consisted mainly of current at the inner segment and was recorded by measuring voltage $-j_3 R_3$.

In bright light the membrane conductance of the outer segment became very low, but the exact value could not be satisfactorily determined because small errors in the adjustment of the leakage compensation changed the apparent conductance by up to several pS.

Because of slow drift, the absolute value of the current collected by the suction electrode was measured indirectly, by assuming the level at the top of the saturating light response to be zero when current was not being injected (see Baylor, Lamb & Yau, 1979). Drift was then allowed for by frequent measurements of the saturating response and linear interpolation.

Signals were recorded on an FM tape recorder (Ampex PR2200) and digitized, stored and analysed in a PDP 11/34 computer.

Spatial uniformity of voltage control

The following considerations suggest that in the steady state the rod interior was approximately isopotential under voltage clamp. Attwell & Wilson (1980), using the figures of Brown, Gibbons & Wald (1963) for ciliary dimensions and assuming a specific internal resistance of 200 Ω cm, estimated the longitudinal resistance of the cilium as 12 MΩ. Since the largest longitudinal currents we measured were less than 3×10^{-10} A, the largest voltage drop in the cilium should have been less than 4 mV. Voltage attenuation within the outer segment should also have been small. Assuming that the diameter of the outer segment is 10 μm, that 99% of the cross-sectional area is obstructed by internal disks (e.g. Lamb, McNaughton & Yau, 1981), and that the cytoplasm has a specific resistance of 100 Ω cm, the internal resistance, r_i is $1{\cdot}3 \times 10^{10}$ Ω cm^{-1}. The membrane slope resistance r_m ranged between about 10^8 Ω cm at voltages negative to −30 mV and $1{\cdot}5 \times 10^6$ Ω cm at large positive voltages so that the length constant, $\sqrt{(r_m r_i)}$, would have varied between about 30 and 3 times the outer segment length. Treating the outer segment as an unterminated cable (e.g. Jack, Noble & Tsien, 1975) it can be shown that the outer segment would be effectively isopotential for voltages negative to −30 mV. For large positive voltages the distal tip of the outer segment would be a few mV less positive than the base.

Experimental procedure

The positions of the cell and the three electrodes are shown schematically in Fig. 1. The outer segment of an isolated rod on the bottom of the chamber was drawn into the suction pipette and raised to the intracellular electrode tips about 0·5 mm above the bottom. The cell was adjusted in the suction electrode so that the inner segment protruded entirely outside the electrode tip, usually leaving about half of the outer segment inside it. This ensured that 'outer segment' currents were not contaminated by currents at the inner segment. The inner segment was next positioned directly under the tips of the intracellular electrodes, the microscope condenser focused, and the leakage current compensation adjusted.

The second intracellular electrode was inserted after the rod had recovered from penetration by the first. Good penetrations caused little change in the light-sensitive current. The cell recovered from penetration over a period of a few minutes, as judged by a gradual increase in the resting potential and amplitude of the saturating voltage response. Recovery was sometimes helped by adjusting the vertical position of the intracellular electrode.

Experiments were continued only if the light responses measured by both intracellular electrodes were identical. Occasionally the two responses differed in amplitude by a factor of up to two, apparently because of a voltage divider network at the tip of the electrode giving the smaller response. A divider might arise if the electrode 'dimpled' the membrane while failing to penetrate it completely, or if there were a longitudinal crack in the tip of the electrode. Sometimes adjustment of the position of the electrode in the cell eliminated the divider effect.

Solutions

The Ringer solution contained (mM): NaCl, 111; KCl, 2·5; $MgCl_2$, 6·0; $CaCl_2$, 1·5; HEPES buffer 3·0 at pH 7·6; EDTA, 0·02; D-glucose, 10. Elevated [Mg] was found to facilitate sealing of the intracellular electrodes in the membrane, and EDTA was added to chelate trace heavy metal contaminants. In some experiments 5 mM-TEA chloride (Kodak) was added to the Ringer solution to reduce a delayed outward-going rectification which otherwise made it difficult to clamp the potential positive to zero. For example, after a voltage step to near 0 mV an outward current activated with a time constant of roughly 50 ms and reached a level of 1–5 nA. This outward current presumably passed through the inner segment, since it was not seen in records of outer segment current. TEA reduced the delayed outward current at the inner segment to a few hundred pA and had no obvious effect on the currents at the outer segment (see Results).

In two experiments the external Ca bathing the outer segment was lowered by perfusing the inside of the suction electrode while the cell was in place, using a back-to-back syringe arrangement (e.g. Hodgkin & Keynes, 1955) suggested by Dr Peter McNaughton. Ringer solution without added Ca and with 2 mM-EGTA was perfused into the tip of the suction electrode through a fine polyethylene tube while an equal volume of solution was withdrawn from the back of the electrode. A second small tube containing normal Ringer solution was used in the same way to restore the [Ca] to normal.

RESULTS

Comparison of photocurrents with voltage freely changing or clamped

Fig. 3 shows flash responses recorded from a rod while the voltage was allowed to change freely and while it was clamped at the dark level of −34 mV. The voltage responses in *A* are very similar to responses of rods in the intact retina (e.g. Schwartz, 1973; Brown & Pinto, 1974; Detwiler, Hodgkin & McNaughton, 1980) and show the prominent initial spike in the response to a strong flash. Voltage responses to weak flashes reached their peak earlier than the current responses because of high-pass filtering by the rod membrane (see Detwiler, Hodgkin & McNaughton, 1978, 1980; Attwell & Wilson, 1980; Baylor *et al.* 1984). The voltage trace in *B* was recorded during presentation of the brightest flash and shows a residual response less than 1 mV in amplitude; smaller errors were present when the flash was dimmer. The similarity of the outer segment currents measured with the voltage clamped or changing is striking and indicates that during a normal flash response the change in transmembrane voltage has little effect on current generation. This explains the finding that the photocurrent recorded from a rod in a piece of retina showed little dependence on the number of receptors illuminated (Baylor *et al.* 1979), even though the voltage response of a rod in the network of coupled cells depends strongly on the number of cells stimulated (e.g. Schwartz, 1976; Gold, 1979, 1981; Detwiler *et al.* 1978, 1980).

The upper records in Fig. 3*B* are total clamping currents. These have the same

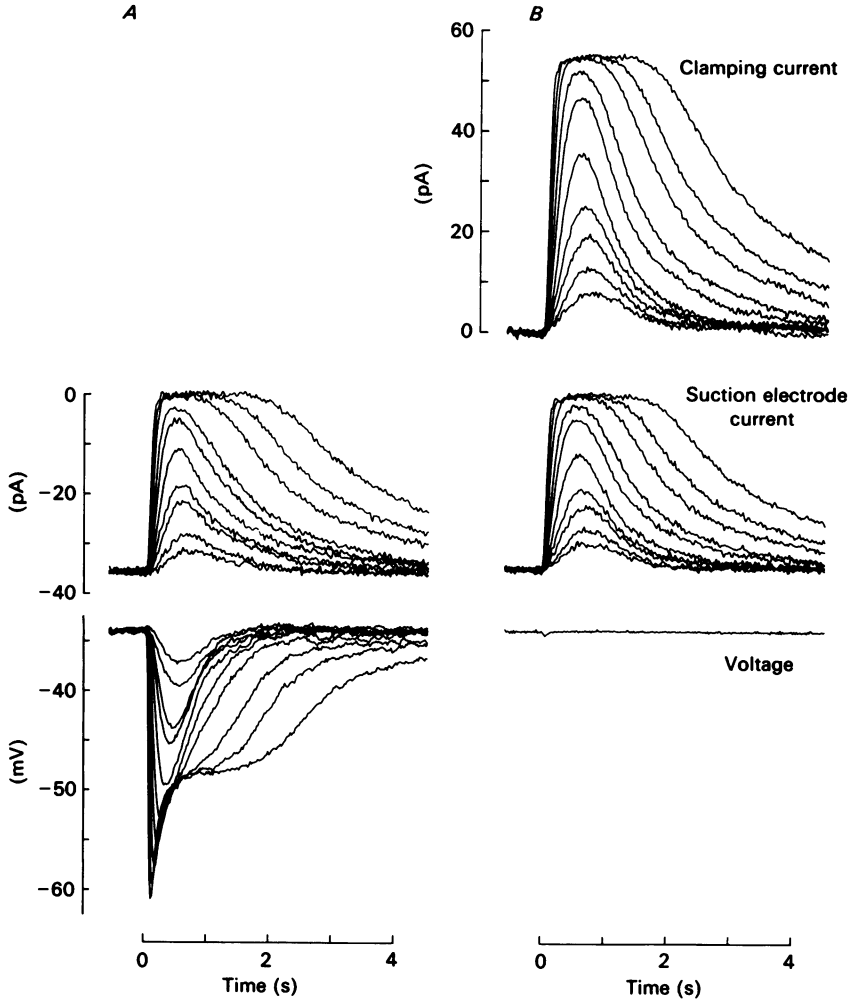

Fig. 3. Superimposed responses to brief flashes of increasing strength with the cell voltage unclamped (*A*) or clamped at the dark level of −34 mV (*B*). Upper traces in *A* are suction electrode currents (with outward current upwards). Lower traces in *A* are voltage responses recorded simultaneously with the currents. Middle traces in *B* are suction electrode currents, upper traces total membrane currents. Bottom trace in *B* is the voltage during presentation of the brightest flash, residual response < 1 mV. Single responses; 11 ms flashes of unpolarized light at 500 nm, delivered at time $t = 0$, photon densities increased by factors of about 2 between 1·5 and 430 photons μm^{-2}. Current low-pass filtered at 20 Hz, voltage low-pass filtered at 30 Hz. Sampling interval, 20 ms, selected to avoid undersampling. Temperature 20·4 °C. Normal Ringer solution without TEA. Cell No. 3 of Table 1. Currents shown in subsequent Figures are those collected by the suction electrode.

form as the currents recorded by the suction electrode but a larger amplitude since the suction electrode collected from only the distal portion of the outer segment.

Table 1 summarizes several parameters of the flash responses from similar experiments on five cells. In each experiment the photocurrents recorded by the

suction electrode were similar with the voltage freely changing and clamped, as in Fig. 3. The flash sensitivities in the right-hand columns of Table 1 were calculated from the peaks of the voltage and current responses to dim flashes. The largest voltage response observed from a rod with two intracellular electrodes in it was 36 mV.

TABLE 1. Parameters of rod flash responses with voltage clamped or not clamped

			R_{max}			t_{peak}		S_F^D	
Cell	T (° C)	V_D (mV)	ΔV (mV)	Δj_c (pA)	Δj_s (pA)	(ΔV) (s)	(Δj_s) (s)	ΔV (mV photon^{-1} μm^2)	Δj_c (pA photon^{-1} μm^2)
1	19·0	−39	> 16	49	12	0·55	0·71	0·39	1·40
2	19·8	−33	> 15	70	14	0·79	0·90	0·44	2·40
3	20·4	−34	27	55	35	0·60	0·72	1·67	5·30
4	17·6	−39	18	45	22	0·62	0·80	0·84	1·73
5	18·3	−40	23	55	14	0·50	0·76	0·57	1·70

Responses were recorded with the voltage changing freely or held at the dark level. V_D is the resting potential in darkness. R_{max} is the amplitude of the saturating response to a bright flash: ΔV is the amplitude of the unclamped photovoltage, Δj_c the saturating photocurrent with voltage clamped, Δj_s the saturating current measured by the suction electrode (similar with voltage clamped and not clamped). t_{peak} is the time-to-peak of the response to a dim flash, measured from records of unclamped voltage response (ΔV) or from suction electrode current response (Δj_s). S_F^D is the ratio of the peak amplitude of the response to a dim flash divided by flash photon density (λ = 500 nm), calculated from unclamped voltage response (ΔV) or clamping current (Δj_c). T is temperature.

The experiments shown in Fig. 4 were performed in order to make a more detailed comparison of clamped and unclamped flash responses. Flashes of fixed intensity were applied in interleaved trials with the voltage clamped or allowed to change. The continuous traces in Fig. 4*A* show the average responses in clamp, the dotted traces the unclamped responses. Fig. 4*B* shows similar results from another rod stimulated

Fig. 4. Comparison of outer segment photocurrents with voltage clamped at the dark level of −34 mV (continuous traces) or changing freely (dotted traces). 11 ms flashes were delivered at time 0 and responses were averaged from interleaved trials. Results in *A* and *B* are from rods 4 and 5 of Table 1 respectively. In *A* and *B* the flash photon densities (500 nm) were 33 and 5 μm^{-2} respectively, responses were averaged from 7 and 20–22 trials respectively. Current low-pass filtered at 20 Hz in *A* and 10 Hz in *B*. Both experiments in normal Ringer solution. Current and voltage plotted relative to the dark levels. *C*, calculated effect of photovoltage on photocurrent for experiment in *B*, with traces corresponding to those in *B*. Wave forms of clamped photocurrent and photovoltage obtained by fitting experimental records. Photocurrent with voltage changing was calculated by convolving the photovoltage with the outer segment's response to a voltage impulse and adding this to the photocurrent under voltage clamp. Details of fitting: photocurrent in clamp fitted by the Poisson expression of eqn. (8) with n = 4 and values of α and k to give a peak response of 2·9 pA at 0·77 s. Voltage fitted by Independence expression of Baylor, Hodgkin & Lamb (1974, eqn. (41)) with n = 5 and values of k and α to give a peak response of −3·2 mV at 0·49 s. Response to a voltage impulse obtained by differentiating the response to a 20 mV hyperpolarizing step, delivered shortly after obtaining the records in *B*. The response to the step consisted of a current relaxation 2·8 pA in size with the form of eqn. (7), α = 3 s^{-1}. The decrease in photocurrent, obtained by convolving the derivative of this expression with the voltage wave form, reached a maximum of 0·25 pA at 1·06 s after the flash.

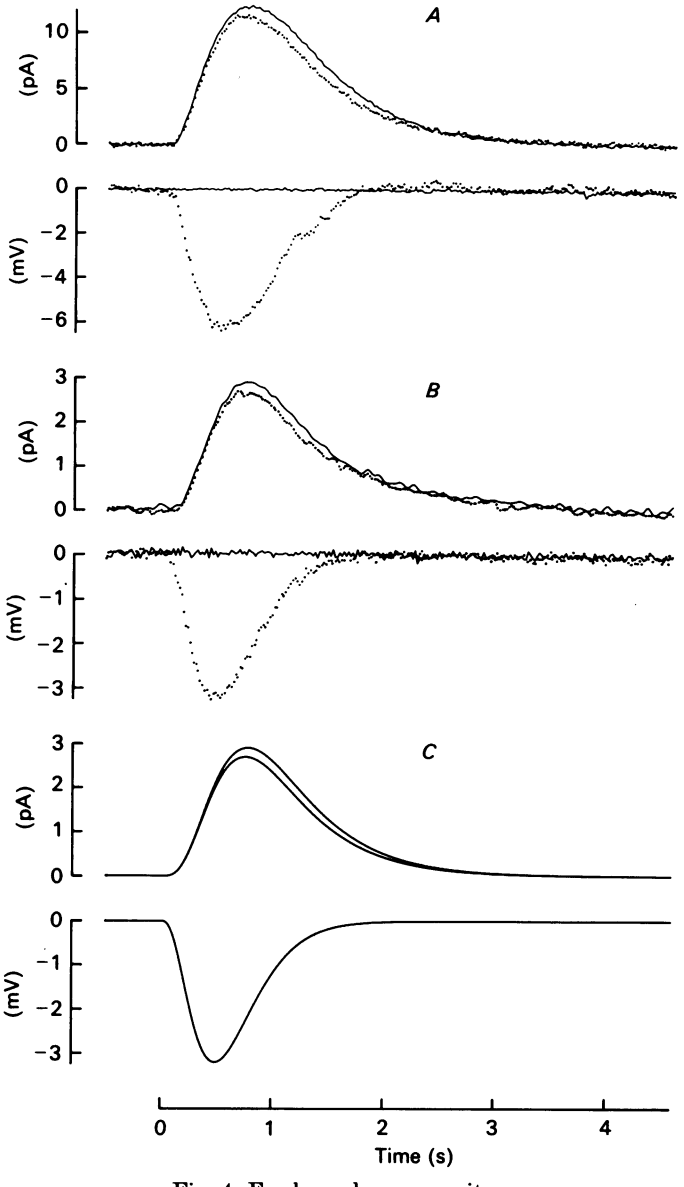

Fig. 4. For legend see opposite.

by a weaker flash. In each experiment the two photocurrents began to rise along the same curve but then diverged, the clamped response becoming slightly larger. The peak difference between the clamped and unclamped responses occurred well after the peak hyperpolarization. This indicates that the voltage change had little instantaneous effect on the photocurrent but reduced it after a lag. The basis of this effect is examined on p. 136 (see also Fig. 4*C*).

The conclusion from these experiments is that the rod's voltage response has only a small, delayed effect on the generation of the photocurrent.

Reversal potential of light-sensitive current

Fig. 5 shows a rod's responses to saturating flashes when the voltage was held at the dark level of −31 mV or changed to other levels for periods of 20 s. Hyperpolarization to −61 mV caused a slow increase in inward current, and the light

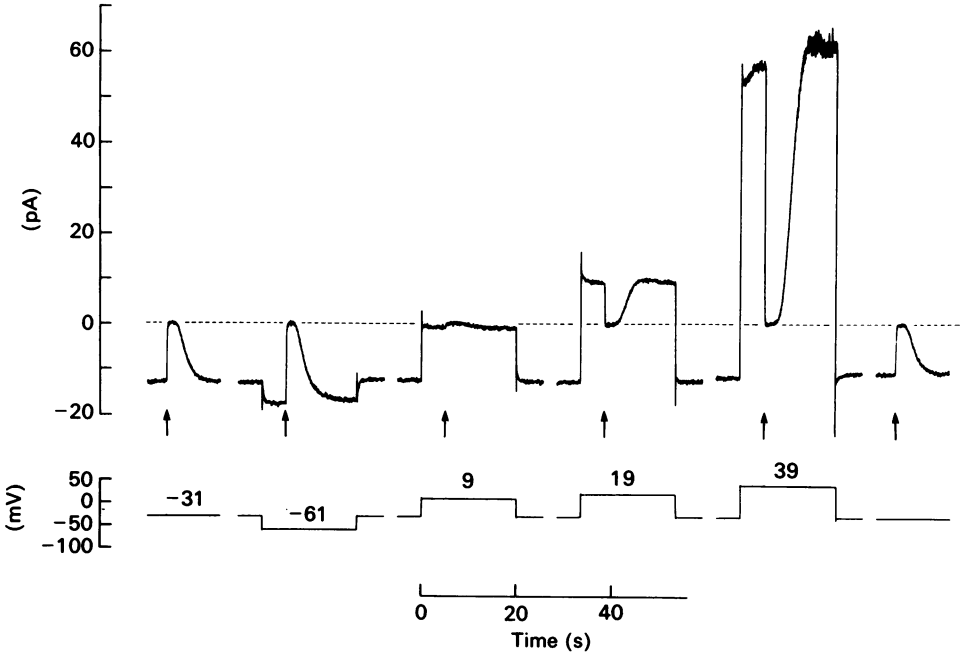

Fig. 5. Dependence of dark current and saturating photocurrent on steady-state voltage. Absolute current collected by suction electrode plotted above, with zero level shown by dotted line; recorded voltage plotted below. Potential was held at the dark level of −31 mV or changed to the level indicated for a period of 20 s. Saturating flashes (260 photons μm^{-2} at 500 nm) delivered at times shown by arrows. Voltage and current low-pass filtered at 15 Hz. 5 mM-TEA added to Ringer solution; temperature 21 °C; peak voltage response to a bright flash 21 mV.

response, which completely abolished the inward current, was larger. Depolarization to +9 mV reduced the light-sensitive current to about 1 pA, and the current became outward for stronger depolarizations. Depolarization also prolonged the flash response, an effect examined further on p. 138. The experiment gives the reversal potential of the light-sensitive current as about +10 mV and shows that the conductance of the outer segment became very small during the saturating response, since the absolute current at the plateau of the light response was near zero at all values of potential. Similar results were obtained in several other experiments.

'Instantaneous' current–voltage relation of light-sensitive conductance

Fig. 6 shows current–voltage relations from an outer segment in darkness and in steady light of half-saturating or saturating intensity. The inset shows the methods of determining the relation. The voltage was held at the dark level of −31 mV and

then abruptly changed to a different level for 50 ms. Voltage and current were averaged over a 20 ms time window that began when the voltage and current had settled (roughly 10 ms after the onset of the voltage step). There was no evidence of a relaxation in current during the window, and averaging over it improved

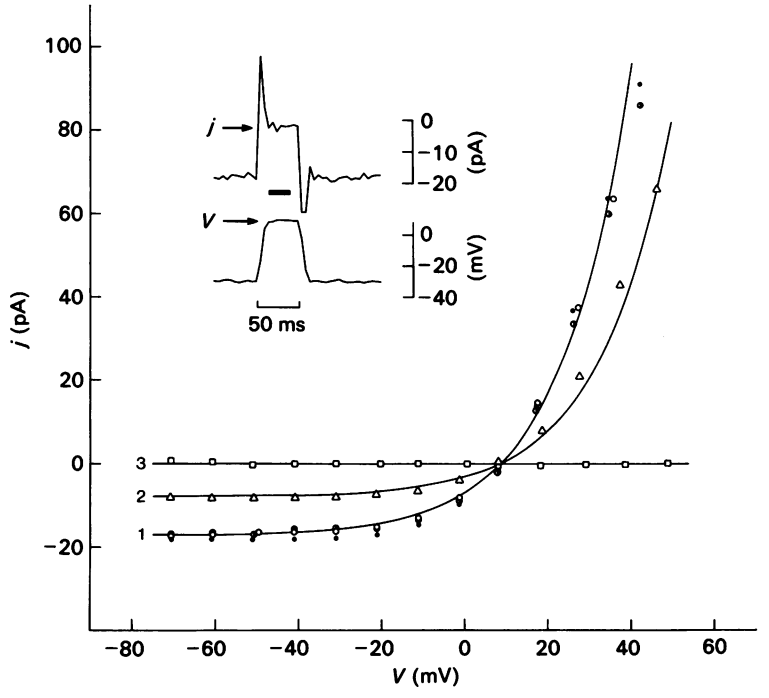

Fig. 6. Instantaneous current–voltage relations of outer segment membrane in darkness (curve 1) half-saturating light (2) and saturating light (3). Voltage was held at the dark level of −31 mV and changed to other levels for 50 ms. j is the current measured by the suction electrode after making the step to voltage V. Inset: sample records from a step to +9 mV in darkness and method of measuring current and voltage; traces averaged from two sweeps. Heavy bar shows time window over which current and voltage were measured and averaged. Capacity spike for the negative-going voltage change was truncated. Sequence of runs was: ○ (dark), △ (half-saturating light), ● (dark), □ (saturating light), ◑ (dark). Each point is the average from several sweeps. Relation (3) in saturating light fitted with a straight line of slope 0·8 pS at zero current. Relations (1) and (2) drawn according to eqn. (2) of text with V_r = +8·5 mV, b = 17·0 mV, and j_N = −17·5 pA (dark) or −8·0 pA (half-saturating light). 5 mM-TEA Ringer solution, same rod as in Fig. 5. Initial resistance of the cell measured by a small current step was 750 MΩ in dark, time constant of voltage relaxation after a current step was 40 ms. Outer segment current low-pass filtered at 100 Hz, sampling interval 5 ms. Steady intensities at 500 nm were: 15 photons $\mu m^{-2} s^{-1}$ (curve 2) and 6750 photons $\mu m^{-2} s^{-1}$ (curve 3).

resolution. This type of current–voltage relation, determined at a fixed early time roughly 20 ms after changing the voltage, will be termed 'instantaneous'. The relation in the dark (curve 1) was strongly outwardly rectifying, with a region of nearly constant inward current at potentials negative to −20 mV and a region of increasing outward currents at potentials positive to +20 mV. The reversal potential

was near +8·5 mV. The average reversal potential estimated in this way from experiments on eight rods was 8±4 mV (±S.D.), or 5±4 mV if corrected for the change in tip potential of the voltage electrode (see Methods). In one experiment without TEA the uncorrected reversal potential was near +5 mV. These values for the reversal potential are in agreement with those reported by Bader *et al.* (1979) and MacLeish *et al.* (1984).

In bright light (curve 3) the current–voltage relation was flat. The slope of the straight line fitted to the points by linear regression gives an estimate for the membrane conductance of 0·78 pS. In another similar experiment the conductance in bright light was estimated as 6·2 pS. These values are somewhat uncertain because they depend on the adjustment of the leakage compensation circuit (see Methods). In earlier experiments without the compensation circuit, the leakage current was estimated and subtracted using the method of Baylor *et al.* (1984), and the apparent slope conductance in bright light ranged from 0·6–33 pS (average 16·2±10 pS, S.D., $n = 8$). In three of these experiments TEA was not added to the Ringer solution, so that the low conductances did not result from a TEA block of light-insensitive channels in the outer segment. Indeed, the results support the interpretation that light-sensitive channels comprise the main or exclusive ionic conductance of the outer segment (Baylor & Lamb, 1982; Baylor *et al.* 1984).

In steady light of half-saturating intensity (curve 2) the current–voltage relation had the same form as the relation in the dark but the currents were smaller. This is brought out by continuous curves 1 and 2, which have the same form and reversal potential and differ only in their vertical scaling. This simple change in the scaling of the currents is expected if light blocked half the channels without changing the ionic concentration gradients or the rectification characteristic of an open channel.

A quantitative description of the current–voltage relation can be obtained with the barrier rectification equation (Jack *et al.* 1975) applied to rods by Bader *et al.* (1979). This model, which has the virtue of simplicity, assumes that the rectification depends on a 'bottleneck' that limits the inward current through the channel at negative potentials. If the current is carried by ions with a valence z and there is a single energy barrier located at a fractional distance γ from the inner surface of the membrane, the form of the current–voltage relation should be given by (Jack *et al.* 1975, p. 232)

$$j(V) = A\,[\exp(zF\gamma V/RT) - B\exp(-zF(1-\gamma)\,V/RT)]. \quad (1)$$

Here $j(V)$ is the current measured at voltage V just after changing the voltage from the holding level, A is a constant of proportionality, and F, R and T have their usual meanings. The constant B is determined by the reversal potential V_r of the current according to $B = \exp(zFV_r/RT)$. It will be shown that this equation fits the results if $\gamma = 0{\cdot}99$, which is appropriate for a barrier very near the outer surface of the membrane. For this case, eqn. (1) can be approximated by

$$j(V) = j_N\,[1 - \exp((V - V_r)/b)], \quad (2)$$

where j_N is the value of j at large negative V and the exponential steepness parameter b is given by RT/zF.

Parameters V_r and b of eqn. (2) were estimated by making semilogarithmic plots of the current–voltage relations. Collected results from three cells are shown in

Fig. 7, with the current scaled as $(j-j_N)/(-j_N)$ and plotted on a logarithmic scale as a function of V. The straight lines provide a satisfactory fit over most of the range although the points fall below the lines at large outward currents. This deviation may result from a saturation in the channel or from failure of the outer segment to remain isopotential during strong depolarizations. The slopes of the lines give values of $1/b$

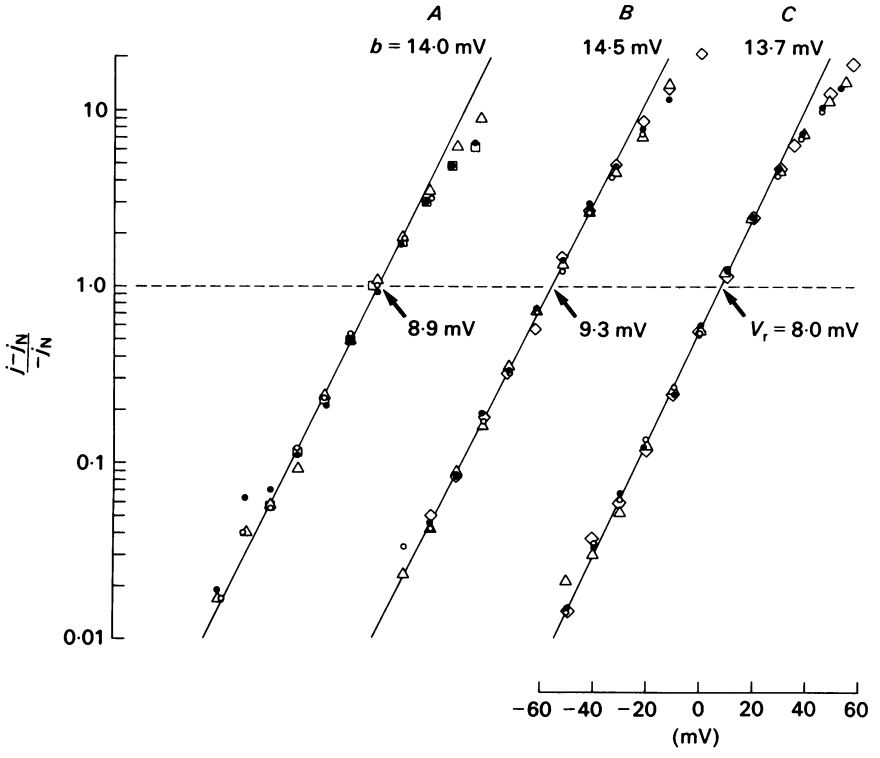

Fig. 7. Instantaneous current–voltage relations of outer segment determined as illustrated in Fig. 6 and plotted on semilogarithmic coordinates. Collected results from three cells. Ordinate is normalized outer segment current $(j-j_N)/(-j_N)$. Straight lines fitted by eye represent the barrier rectification model of eqn. (2), with values of reversal potential V_r and rectification parameter b as indicated. Voltage scale applies to the right-hand set of points (*C*); results from the other two cells have been displaced to the left for clarity. Different symbols represent runs in darkness or steady 500 nm lights of various intensities up to roughly half-saturating. Light intensities (photons $\mu m^{-2} s^{-1}$) and values of $-j_N$ (pA) were, in sequence, cell *A*: ○ dark, 17·3; △ 15, 8·6; □ dark, 17·8; ● dark, 17·1, cell B: ○ dark, 12·0; △ 4·4, 10·6; ◇ 53, 6·0; ● dark, 9·8 and cell *C*: ○ dark, 16·4; △ 8·9, 10·3; ◇ 31, 7·6; ● dark, 15·1. Cell *A* is same rod illustrated in Figs. 5 and 6. TEA Ringer solution in each experiment.

while their positions give values of the reversal voltage V_r. Different symbols plot results obtained in the dark and in various levels of steady light. The points from a given rod fell along the same curve, demonstrating again that light scaled the currents without altering b or V_r.

The barrier equation often did not fit the current–voltage relation at large outward currents (e.g. Fig. 7), and so the best choice of the rectification parameter b was

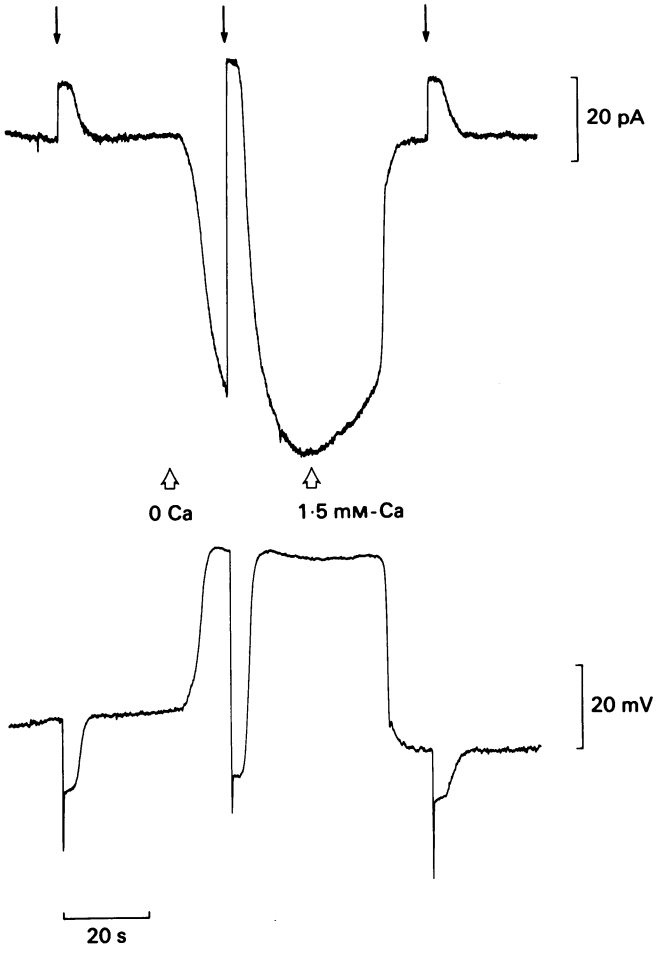

Fig. 8. Effect of lowering Ca concentration in suction electrode on rod voltage (lower trace) and outer segment current (upper trace). Saturating flashes delivered at arrows. During the period indicated the Ca concentration in the tip of the suction electrode was lowered by perfusing 0 Ca Ringer containing 2 mM-EGTA through it with back-to-back syringes. Return to normal Ringer was effected by perfusing control solution containing 1·5 mM-Ca. Large arrows show times of advancing the perfusion syringe: the timing of the solution changes at the outer segment is uncertain. The different saturating levels of the current responses to light flashes are explained by a junction current on introducing 0 Ca, 2 mM-EGTA Ringer solution (Hodgkin *et al.*, 1984). 5 mM-TEA Ringer solution bathed the inner segment. Current low-pass filtered at 10 Hz, voltage at 30 Hz. Temperature 21·2 °C.

somewhat arbitrary and depended on the kind of curve to be fitted. Semilogarithmic plots place more emphasis on the inward currents and required somewhat smaller values for b than linear plots. For example, the results in the linear plot of Fig. 6 were fitted by taking $b = 17$ mV, while the same results on semilogarithmic plots (Fig. 7*A*) were fitted by $b = 14$ mV.

At large negative potentials the inward currents did not reach the nearly constant value implied by eqn. (2), but instead showed a small linear increase with increasing

hyperpolarization. For the rods of Fig. 7*A*, *B* and *C*, the slopes of this linear component at voltages negative to −40 mV were 47, 25 and 29 pS respectively. In bright light the corresponding slopes were 4·7, 0·1 and 3·8 pS, so that the dark slopes did not arise from error in the measurements. Although eqn. (2) predicts a slope of 0·01 pS over the same region, a finite slope similar to that actually observed is predicted by eqn. (1) with $\gamma = 0{\cdot}99$ and $z = 2$. With this value of γ, eqn. (1) gives a relation that is nearly identical to that from eqn. (2) at potentials positive to −60 mV. Semilogarithmic plots of current–voltage relations, such as those in Figs. 7 and 11, were restricted to the voltage region positive to −60 mV where the simplified model gives a good description.

The average value of the steepness parameter b determined from semilogarithmic plots of the current–voltage relations as in Fig. 7 was 14 ± 2 mV ($\pm$S.D., $n = 11$). A similar value ($12{\cdot}2 \pm 2$ mV, S.D.) was found in five experiments without TEA, where only the region negative to 0 mV could be studied. This is a steeper exponential dependence than that reported by Bader *et al.* (1979), who found b to be 25 mV. Within experimental error the value of b observed here is that expected for $z = 2$. On the barrier model of the rectification this implies that the current carriers are doubly charged.

We conclude that the current–voltage relation measured 10 ms after switching the voltage is fitted by eqn. (1) with $\gamma = 0{\cdot}99$ and $z = 2$. Light appears to scale the number of open channels by a mechanism that is voltage insensitive on a short time scale. In saturating light few channels of any type (light-sensitive or light-insensitive) remain in the conducting state.

Current–voltage relation with reduced external Ca

The effects of low external [Ca] on the current–voltage relation were examined in two experiments by perfusing the inside of the suction electrode using back-to-back syringes (see Methods).

Fig. 8 shows that on removal of external Ca the inward current increased and the intracellular voltage rapidly depolarized (voltage not clamped). These changes, as well as the increased amplitudes of the flash responses, are similar to the effects reported by Hagins & Yoshikami (1977), Yau, McNaughton & Hodgkin (1981) and Bastian & Fain (1982). Fig. 9 shows the current–voltage relations determined before, during and after exposure to low $[Ca]_o$. The main effect of removing external Ca was simply to increase the current at each voltage. There was no change in the reversal potential in low $[Ca]_o$, suggesting that the ionic selectivity of the light-sensitive channel and the internal ionic concentrations were unaltered. The constancy of the reversal potential also suggests that Ca is not a major carrier of the dark current under normal conditions. The current–voltage relation in low $[Ca]_o$ still showed outward rectification, as reported by MacLeish *et al.* (1984). Thus it seems unlikely that the rectification observed in normal $[Ca]_o$ can depend entirely on a simple voltage-dependent block of the light-sensitive channels by external Ca. In low $[Ca]_o$, however, the rectification was somewhat less steep than that in normal Ringer solution, suggesting that external Ca may play some role.

The currents measured on return to normal $[Ca]_o$ (squares, Fig. 9) were roughly half those measured before removal of external Ca. Such a reduction of current

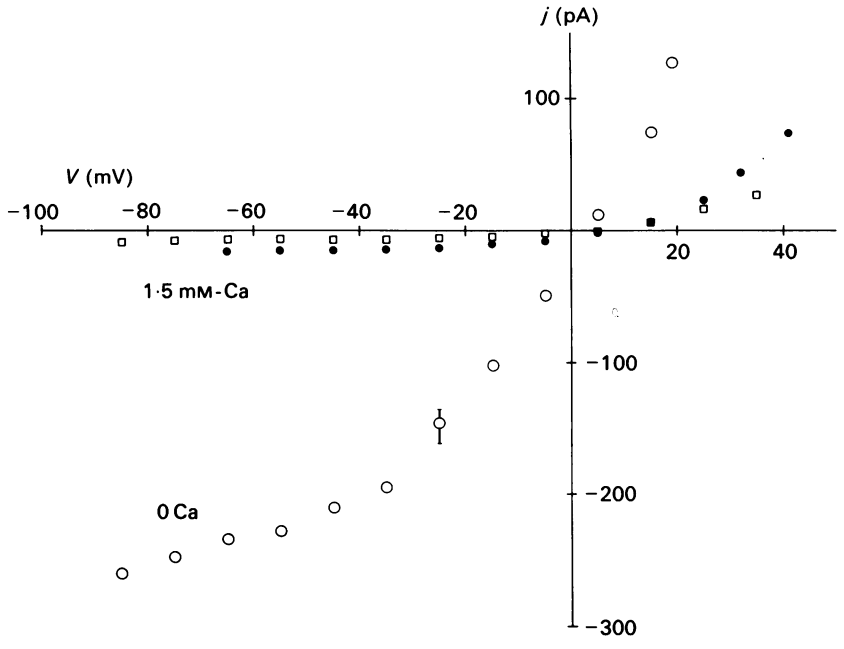

Fig. 9. Effect of removal of external Ca on instantaneous current–voltage relation of outer segment. Different symbols show relations determined sequentially in: ● – normal-Ca Ringer, ○ – low-Ca Ringer (nominally 0 Ca with 2 mM-EGTA), □ – normal-Ca Ringer solution. The measurements in low Ca were made in 30 s; during this time the light-sensitive current declined from −160 to −135 pA at the dark voltage (shown by the bar at −25 mV). Same cell illustrated in Fig. 8.

following a build up of internal Na in low-$[Ca]_o$ solutions has been reported by Yau *et al.* (1981) and Hodgkin *et al.* (1984).

Lowering $[Ca]_o$ gave similar effects on the current–voltage relation of another rod.

Slow voltage-dependent relaxations of light-sensitive current

Previous current-clamp experiments (Baylor *et al.* 1984) suggested that the light-sensitive conductance slowly relaxes when the voltage is changed. The experiments illustrated in Fig. 10 show this effect in voltage clamp. The traces are outer segment currents recorded from two rods during long voltage steps given in integral multiples of 10 mV. Hyperpolarizations caused a slow, graded increase in dark current, while depolarizations caused a reduction. The relaxations did not occur in bright steady light, so that they represent changes of current in the light-sensitive channels.

Comparison of 'instantaneous' current–voltage relations obtained from various holding levels showed that the slow relaxation involved a change in only the amplitude of the current, the reversal potential V_r and rectification parameter b of eqn. (2) remaining constant. This is illustrated in Fig. 11 where currents scaled as $(j-j_N)/(-j_N)$ are plotted logarithmically as a function of voltage. For a given experiment each set of symbols shows results obtained at a different steady holding voltage. Each set of points falls along the same line, as expected if the holding level determined only the vertical scaling of the instantaneous current–voltage relation.

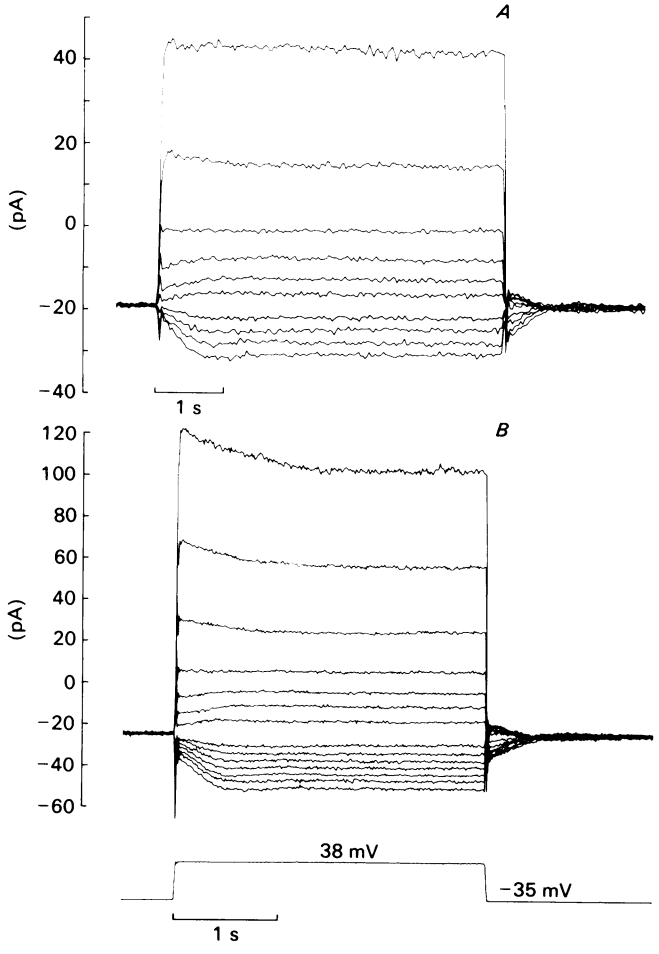

Fig. 10. Records of outer segment current during long displacements of cell voltage from the resting level. Voltage changes in 10 mV steps from resting level. *A*, holding level −32 mV, dark current at rest −19 pA. Low-pass filtered at 15 Hz. *B*, holding level −35 mV, resting dark current −24 pA. Low-pass filtered at 50 Hz. Lower record shows voltage during largest depolarizing step. TEA Ringer solution in both experiments.

This behaviour suggests that the light-sensitive current $j(V,t)$ can be described as the product of a time-independent current $j(V)$ (eqn. (2)), which is proportional to the current–voltage relation of an open channel, and an activation function $y(V,t)$ describing how the fraction of channels open at time t depends on voltage:

$$j(V,t) = j(V)\, y(V,t). \tag{3}$$

If this is so, the steady-state activation curve $y(V,\infty)$ can be obtained from experiments of the kind illustrated in Fig. 10, in which the voltage was held at a steady level V_H and changed to a new level V for a few seconds. If the current measured at V soon after the change is $j(V)$ and the current relaxes to $j(V,\infty)$ at the end of the voltage pulse, then the steady-state activation curve is given by:

$$y(V,\infty) = \frac{j(V,\infty)}{j(V)}. \tag{4}$$

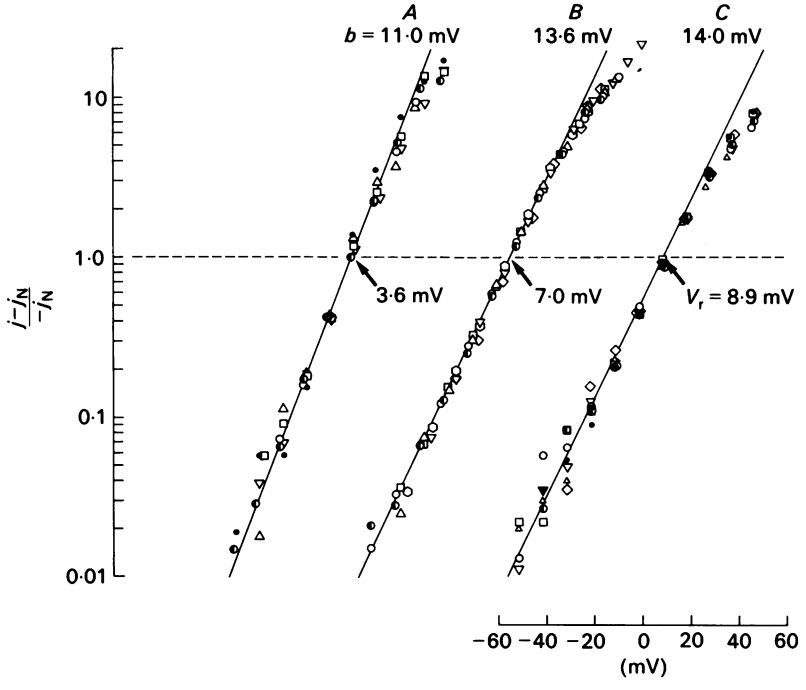

Fig. 11. Instantaneous current–voltage relations of outer segment measured from different holding voltages in darkness. Results from three different rods. Normalized outer segment current $(j-j_N)/-j_N$ plotted on a logarithmic scale as a function of voltage. Each set of symbols denotes a curve determined from a particular holding voltage: ○, ◑, ● are curves determined from −30 mV, these control curves were determined before, during and after determinations from other voltages: ⬡ −70 mV; △ −50 mV; □ −10 mV; ▽ +10 mV; ◇ +30 mV. Reversal potential for cell *A* declined progressively from 3·6 to 2·2 mV, and for cell *B* from 7 to 3 mV. Late curves shifted to the right to make all reversal potentials coincide. TEA Ringer solution in each experiment. Rods *B* and *C* are same as in Figs. 7*C* and 5 (and Fig. 6) respectively.

A second estimate of $y(V, \infty)$ can be made from the currents measured on returning to V_H:

$$y(V, \infty) = \frac{j(V_H)}{j(V_H, \infty)}, \tag{5}$$

where $j(V_H)$ is measured immediately after the return to V_H and $j(V_H, \infty)$ is the steady current at V_H.

This procedure is illustrated in Fig. 12. The filled circles in Fig. 12*A* show the steady-state current–voltage relation $j(V, \infty)$ of the rod of Fig. 10*B*, while the open circles show the instantaneous relation $j(V)$ measured from a holding voltage V_H of −35 mV. The two current–voltage relations cross at V_H and also at V_R, the reversal potential, which in this rod was +3 mV. Fig. 12*B* shows the activation function $y(V, \infty)$ relative to its value at −35 mV, determined from eqn. (4) (open squares) and eqn. (5) (triangles). The activation curve of this rod appears to have a minimum at around 0 mV. Near the reversal potential the activation could not be determined from eqn. (4) because the currents were very small.

For comparing results from different cells the activation curves were normalized to a value of unity at large negative voltages. Normalized activation functions $Y(V, \infty)$ from nine rods are plotted in Fig. 13, which shows that the curves were similar at large negative voltages but varied between cells at positive voltages. In

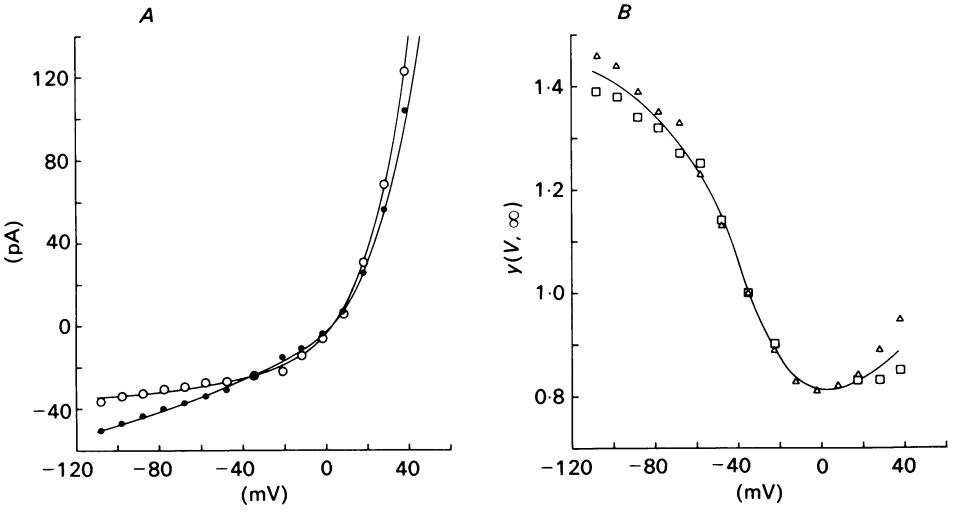

Fig. 12. Instantaneous and steady-state dark current–voltage relations for rod of Fig. 10*B*. *A*, 'instantaneous relation', ○, measured 65 ms after changing voltage from the holding level of −35 mV. 'Steady-state' relation, ●, measured 3 s after step. Continuous curves drawn by eye with reversal potential at +3 mV. *B*, voltage dependence of activation variable $y(V, \infty)$ relative to its value at −35 mV: □ calculated from ratio of steady-state and instantaneous currents in *A*; △ calculated from ratio of instantaneous tail current on returning to −35 mV and steady-state current at −35 mV. Continuous curve drawn by eye.

two rods strong depolarization reduced the current to very low levels, and $Y(V, \infty)$ approached 0·1 at potentials around +20 mV. In the other rods, the value of $Y(V, \infty)$ declined with increasing depolarization between −80 mV and 0 mV but showed little change or rose again at positive voltages. The rise in Y at positive potentials appeared to be characteristic of the 'better' cells. The empirical curves in Fig. 13 were drawn according to:

$$Y(V, \infty) = \frac{1}{1+e^{(V-V_0)/S}} + \frac{d}{1+e^{-(V-V_1)/S}}. \quad (6)$$

The constant V_0 was taken as −21 mV, V_1 as +13 mV, and S as 25 mV. The constant d was taken as 0 for the steepest curve (3), 0·62 for the intermediate curve (2) and 0·97 for the curve showing the least voltage dependence (1). Eqn. (6) provides a rough description of the observations and illustrates the relatively shallow voltage dependence of the gating of the light-sensitive conductance.

The simplest relation, curve 3 in Fig. 13, showed an e-fold change in 25 mV. This behaviour is expected if the gating depends on movement of a singly charged particle across the full thickness of the membrane. On p. 142 we discuss the possibility that

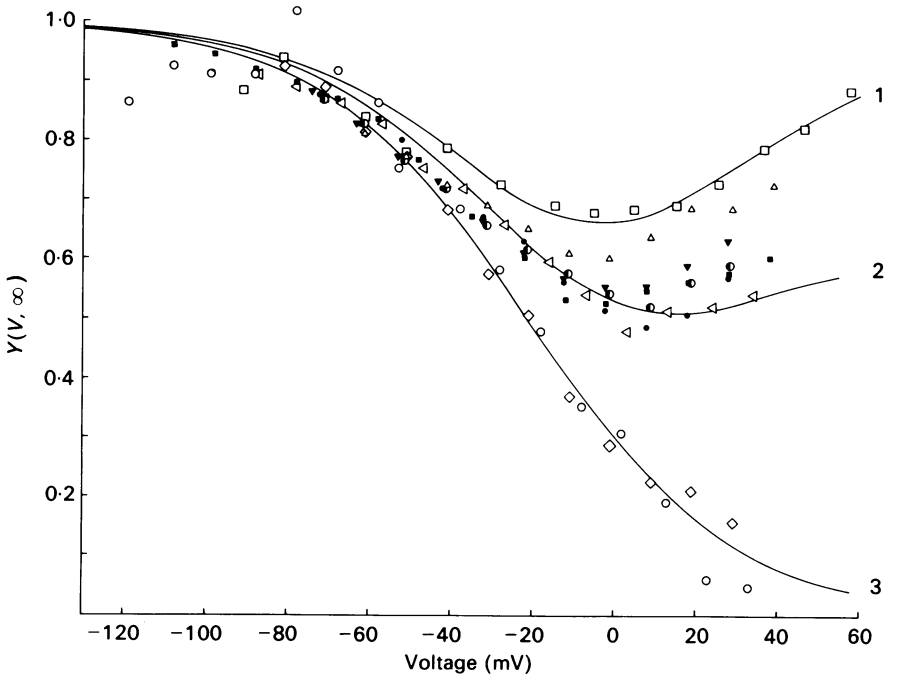

Fig. 13. Normalized steady-state activation functions for the voltage dependence of the light-sensitive current. Collected results from nine rods. Activation was determined as described in text (points are average values from eqns. (4) and (5)) and normalized by the value at large negative potential. Smooth curves drawn according to eqn. (6) of text, with $d = 0{\cdot}97$ (curve 1), 0·62 (curve 2) and 0 (curve 3). Results from rods used in other Figures: △, Fig. 11*C*; ▼, Fig. 10*A*; ■, Figs. 10*B* and 12.

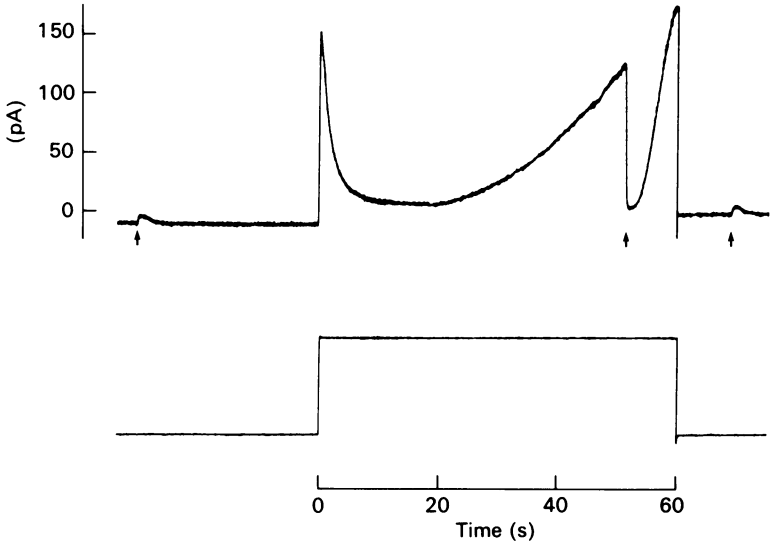

Fig. 14. Collapse and recovery of outer segment current (top trace) during an 80 mV depolarization from the resting voltage; recorded voltage below. Saturating flashes, 722 photons μm^{-2}, delivered at arrows. Photographed from chart record with frequency response 0–150 Hz for small signals.

voltage acts by modulating an electrogenic Na–Ca exchange with a 3–1 coupling ratio, gating the conductance by changing internal Ca.

Activation curves from most cells showed a secondary rise at positive voltages, perhaps reflecting a second process that opens the light-sensitive channels. Results supporting this interpretation are shown in Fig. 14. The upper trace shows the current during a depolarization of 80 mV from rest. The initial outward current rapidly collapsed but then, after a delay of about 20 s, rose again at an increasing rate. This current was light-sensitive as it was blocked by a bright flash. Similar results were obtained from another rod. The initial collapse of the light-sensitive current suggests that these rods would have had activation curves similar to curve 3 in Fig. 13, when measured within a few seconds of a voltage change. The delayed increase in the light-sensitive current in these cells may reflect the slow activation of a process which turns on more quickly in cells with activation curves of the form of (1) in Fig. 13.

Kinetics of relaxation of light-sensitive conductance

After a step change in voltage the light-sensitive current relaxed slowly to the new steady level. In the records of Fig. 10*A* and *B* the initial relaxation of the current was complete in 0·5–0·7 s after a small voltage step, and was followed by a slower sag in the opposite direction. There was an S-shaped delay in the relaxation after the large negative steps in Fig. 10*B*, whereas the initial change in current in Fig. 10*A* could be fitted by either a single exponential or functions with a higher-order delay. Noise made it difficult to resolve the exact form of the rise after small steps. Fig. 15 shows the slow phases of the current changes of Fig. 10*B* after voltage steps of -10 mV and -70 mV (noisy traces) fitted by

$$j(V,t) = c(1-e^{-\alpha t}(1+\alpha t)), \tag{7}$$

where c and α are constants. Eqn. (7) has the form of the step response of the Poisson model of Fuortes & Hodgkin (1964) with two sequential stages of delay each with rate constant α. This provides an adequate description of the initial change in the light-sensitive current after a voltage step. The traces in Figs. 10 and 15 also show a slow rebound of the current after the initial maximum. In eqn. (7) and Fig. 15 this small effect is ignored and the scaling constant c was chosen for a good fit of the initial relaxation.

The form of the slow current relaxation was similar for negative voltage steps and small positive steps. At strongly depolarized voltages the direction and magnitude of the relaxation varied among different rods (compare the relaxations in Figs. 5, 10*A* and *B*) depending on the activation function $Y(V,\infty)$ for each rod (Fig. 13). At positive voltages the relaxation was always slower than at the resting voltage and the relaxation could be fitted either by a single exponential or by eqn. (7). For example, in fitting the slow current relaxation in Fig. 10*B* by eqn. (7), the time constant $1/\alpha$ rose from 140 ms at negative voltages to 500 ms for the largest positive voltage (see Fig. 19*A*). In Fig. 10*A* the relaxation for the second largest positive step was small but clearly slower than that at negative voltages (for which $1/\alpha = 150$ ms).

Effect of voltage-dependent gating on wave form of photocurrent

The slow relaxation of the dark current after a voltage step suggests an explanation for the delayed reduction of the photocurrent after a dim flash when the voltage was not clamped (Fig. 4*A* and *B*). In a linear system the reduction in photocurrent would be given by the effect of a voltage impulse on the dark current convolved with the

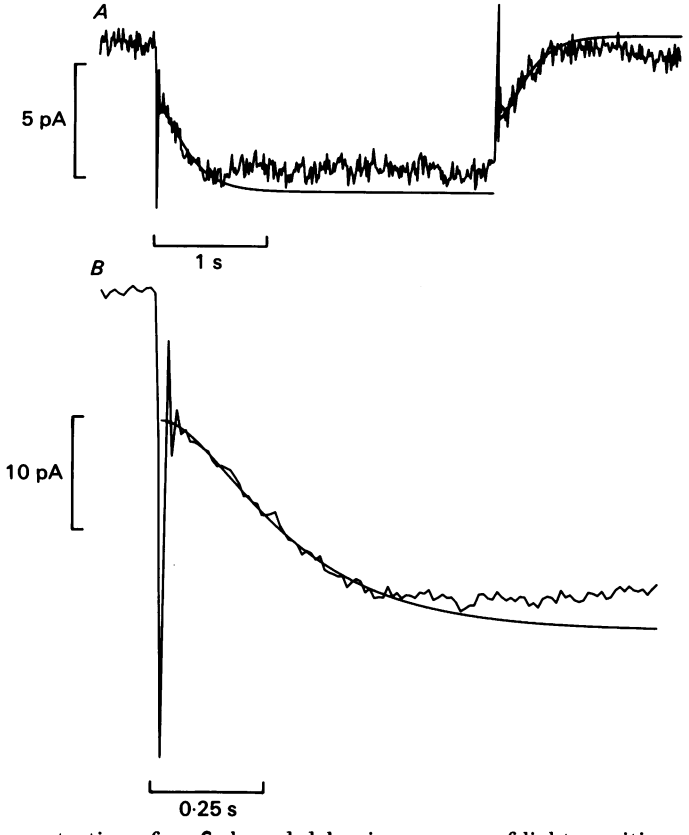

Fig. 15. Demonstration of an S-shaped delay in response of light-sensitive current to a voltage step. Records replotted from Fig. 10*B* for −10 mV step (*A*) and −70 mV step (*B*). Smooth curves have the form of eqn. (7) with $\alpha = 7{\cdot}1\ s^{-1}$ ($1/\alpha = 140$ ms). The forms of the responses to small or large hyperpolarizing steps and to small depolarizing steps were similar.

voltage response to the flash. This was investigated as shown in Fig. 4*C*. The continuous curves in Fig. 4*C* were obtained by fitting the experimental records in Fig. 4*B*. The photocurrent during voltage clamp was fitted by the Poisson expression of Fuortes & Hodgkin (1964) for n stages of rate constant α, as

$$j_f(t) = k(\alpha t)^{n-1} e^{-\alpha t}, \tag{8}$$

where k is a constant proportional to the flash strength and the values of α and n are given in the legend. The voltage response was fitted by the expression mentioned in the legend.

The change in the dark current after a voltage step had the form of eqn. (7) so that the predicted impulse response $j_{\delta V}(t)$, can be obtained by differentiating eqn. (7):

$$j_{\delta V}(t) = c'\alpha^2 t\, e^{-\alpha t}. \tag{9}$$

Here c' is the steady response to a unit voltage step. Eqn. (8) reduces to eqn. (9) when $k = \alpha c'$ and $n = 2$. In using eqn. (9) it is assumed that the slope conductance of the outer segment is small at rest: this was so for the experiment in Fig. 4*B*.

The impulse response of eqn. (9) was convolved numerically with the voltage response in Fig. 4*C* to give the expected decrease in photocurrent:

$$\Delta j(V, t) = j_{\delta V}(t) * V(t), \tag{10}$$

where * represents convolution. The lower current record in Fig. 4*C* is the sum of the photocurrent recorded in voltage clamp and this small decrease Δj, and provides a satisfactory fit to the current response measured out of voltage clamp (Fig. 4*B*). We conclude that the small difference between clamped and unclamped photocurrents is explained by the slow voltage-dependent gating of the current.

Effects of background light on kinetics of current relaxation

Steady dim light speeded the relaxation of the current after a voltage step, in agreement with results presented earlier (Baylor *et al.* 1984). Fig. 16 illustrates the change produced by a steady light of approximately half-saturating intensity. During the light (2) the responses to a voltage step or dim flash were briefer than in the dark (1, 3). When the kinetics of the flash response later slowed down in the dark (4), so too did the relaxation after a voltage step. Similar effects were seen in several other rods.

The parallel behaviour of the kinetics of the flash response and the relaxation after a voltage step is brought out by the smooth curves fitted to the records in Fig. 16. The form of the flash response was fitted by eqn. (8) ($n = 4$), and the response to a voltage step by eqn. (7). The same value for the rate constant α was used for fitting the response to a flash and a voltage step in each condition (dark, light, dark and later in the dark). This is consistent with the idea that a voltage change at the surface membrane evokes an effect that passes through two of the four delays that shape the flash response. Such an interpretation suggests a possible connexion between the relaxation and the 'continuous' component of the dark noise of rods (Baylor, Matthews & Yau, 1980), where the underlying shot effect has the form of eqn. (9).

Voltage dependence of flash response kinetics

Shifting the holding voltage by up to 30 mV negative to the dark level had little effect on the shape of the response to a flash. Strong depolarization, however, slowed the response.

Fig. 17 shows averaged photocurrents recorded from two rods with the voltage clamped at the dark level (continuous traces), and, in interleaved trials, with the voltage 20 mV negative to the dark level (dotted traces). Hyperpolarization increased the size of the dark current and photocurrent by a factor close to 1·27 in each rod; for comparison of wave forms the responses at negative voltage have been scaled down by this amount. In each experiment the shapes of the responses are nearly

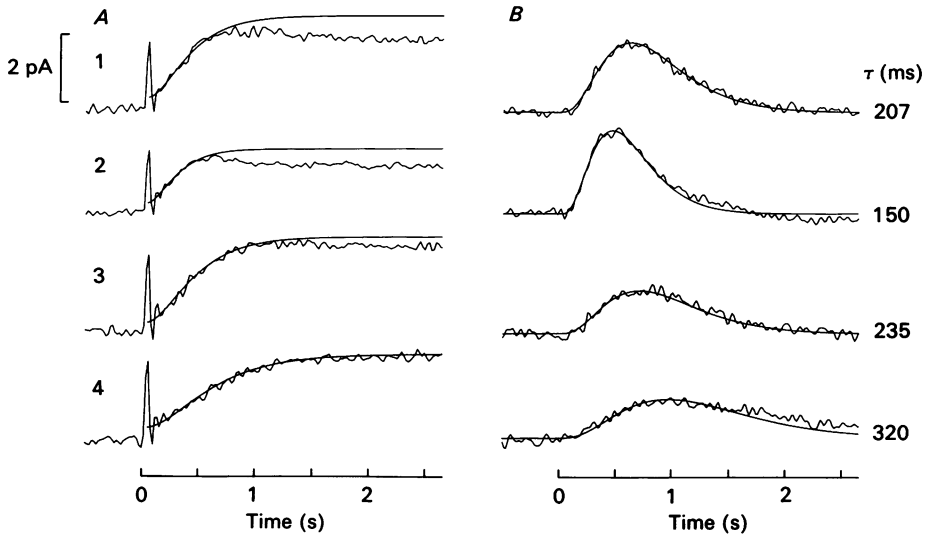

Fig. 16. Parallel effects of a background light on kinetics of voltage-dependent relaxation of light-sensitive current and kinetics of flash response. Left column shows relaxations in current evoked by 10 mV steps in darkness (1), half-saturating background light (2), again in darkness (3) and still later in darkness when the kinetics were slower (4). Right-hand traces show dim flash responses under the four conditions, with flashes given at 0 s. The smooth curves fitted to the slow relaxations in *A* and the flash responses in *B* have the form of eqns. (7) and (8) (with $n = 4$) respectively. In each condition (1–4) the time constants $\tau = 1/\alpha$ (shown on the right) were the same for the response to a voltage step and a flash. The experimental records in *A* are the average of the inverted response to a 10 mV hyperpolarization and the response to a step back to the holding voltage. All records low-pass filtered at 15 Hz and averaged from 6–12 sweeps. Flash photon densities from above downward were 4·0, 42·6, 6·8 and 6·8 μm^{-2}. Intensity of steady light for records in (2) was 632 photons μm^{-2} s^{-1}. Holding voltage level −51 mV; light-sensitive current 34 pA. Normal Ringer solution.

identical, consistent with minimal voltage dependence of the response kinetics. Similar results were obtained in experiments on two other cells.

In each experiment of Fig. 17 the hyperpolarizing step scaled up the light-sensitive current and the photocurrent by the same factor (within 2%) as if light closed the same fraction of light-sensitive channels at both voltages.

Fig. 18 shows the effect of a strong depolarization on the shape of responses to flashes of three strengths. The responses labelled D were recorded when the rod was suddenly depolarized to +29 mV just before the flash, while the other traces were recorded with the voltage at −31 mV. The depolarization reversed the photocurrents; these responses have been inverted and scaled by a single constant that made the amplitude of the saturating response equal to that of the saturating response at −31 mV. The dim flash responses began to rise along the same curve but the response during depolarization reached a larger, later peak and recovered later. Depolarization had the same effect on the response to a brighter flash (middle panel), while for the saturating flash depolarization prolonged the time spent in saturation. There was a definite underswing in all three responses at the depolarized voltage; this feature was

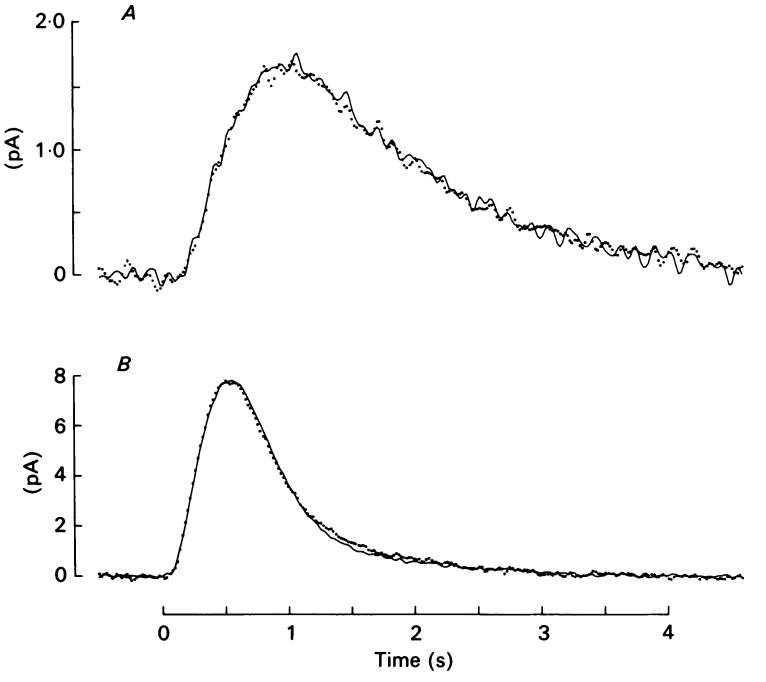

Fig. 17. Lack of effect of hyperpolarization on kinetics of flash response. Averaged current responses recorded from two different rods with voltage clamped at resting potential (continuous curves) or hyperpolarized 20 mV below rest (dotted) in interleaved trials. Hyperpolarization increased the response amplitude and for comparison these responses have been scaled to the amplitude of the current response with voltage clamped at rest. In *A* the resting potential was −40 mV and the saturating response of 11 pA increased to 14 pA with the voltage at −60 mV. Saturating current response measured by the clamping amplifier was 55 pA at −40 mV and flash photon density for the response shown was 5·2 μm^{-2}. Cell 5 of Table 1. In *B* the resting potential was −36 mV and hyperpolarization to −56 mV increased the saturating photocurrent from 36 to 46 pA. Saturating clamp photocurrent was 58 pA. Photon density for response illustrated was 10·5 μm^{-2}. Both experiments in normal Ringer solution.

most pronounced in the saturating response. Depolarization slowed the recovery of the flash response in each of several other experiments. It is important to emphasize that this effect did not depend on a gradual change in the condition of the cell during prolonged depolarization but instead was present immediately after the depolarizing step was applied (time resolution a few seconds). Fig. 19 shows that depolarization had roughly parallel effects in slowing the relaxation of the dark current after a voltage step and the recovery of the response to a bright flash.

DISCUSSION

Instantaneous current–voltage relation

Reversal potential. The reversal potential V_r of the light-sensitive current was about +5 mV after correction for the tip potential of the intracellular electrode (p. 117). This value is consistent with recent evidence that the light-sensitive channel

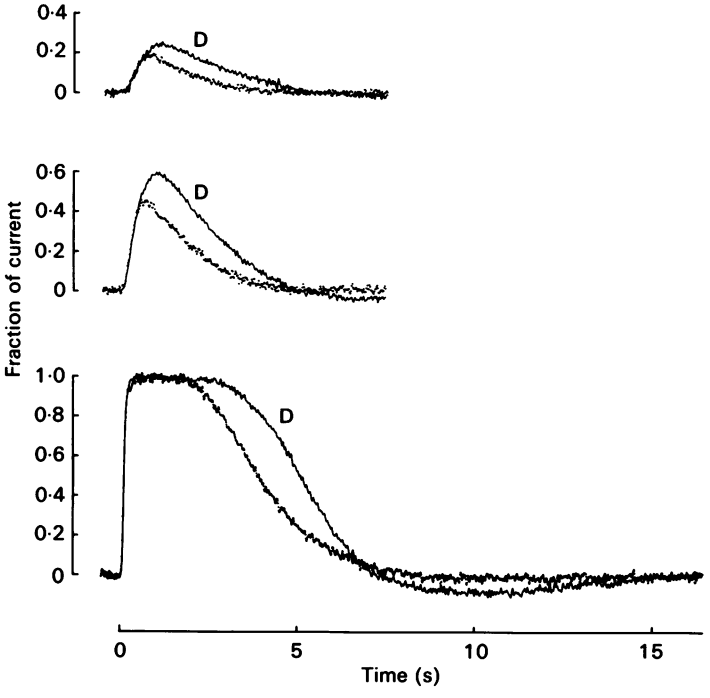

Fig. 18. Effect of strong depolarization on kinetics of photocurrent to flashes of three strengths. Suction electrode currents with voltage clamped at resting level of −31 mV (dotted traces) or at +29 mV (continuous traces labelled D). Response plotted relative to the amplitude of the dark current in each condition; at +29 mV the light-sensitive current was outward and responses were inward. Saturating response amplitudes were +9·1 pA at −31 mV and −35·3 pA at +29 mV. Flash photon densities from above downwards were: 1·9, 6·8 and 261 μm^{-2}. Lowest trace labelled D is a single sweep, other traces averaged from 2 to 8 sweeps. Responses at resting potential were averaged from trials before and after the depolarizations to +29 mV. Low-pass filtered at 15 Hz. TEA Ringer solution.

has a relatively high permeability to K as well as to Na (Capovilla, Caretta, Cervetto & Torre, 1983; Yau & Nakatani, 1984*a*; Hodgkin, McNaughton & Nunn, 1985). If the only appreciable permeability is to these ions and $[K]_i = [Na]_o$, the permeability ratio K/Na calculated by the Goldmann–Hodgkin–Katz equation is $\exp(-V_r F/RT) = 0{\cdot}82$, which is close to the ratio estimated by Yau & Nakatani (1984*a*) and Hodgkin *et al.* (1985).

Outward rectification. The 'instantaneous' current–voltage relation of the light-sensitive conductance was fitted fairly well by eqn. (1). The small but finite slope at very negative voltages was consistent with a barrier located near, but not quite at, the outer surface of the membrane ($\gamma = 0{\cdot}99$). The rectification was rather steep and required a charge z of 2·0 on the current carriers (b in the simple model of eqn. (2) was 13 mV). This value for z is obviously not consistent with the notion that Na and K ions, moving independently, carry most of the current through the light-sensitive channel. On the barrier model, the implication would be that monovalent cations move through the channel only in pairs. Such a coupled movement might occur in a single-file pore occupied by two ions at a time (Hodgkin & Keynes, 1955), or by

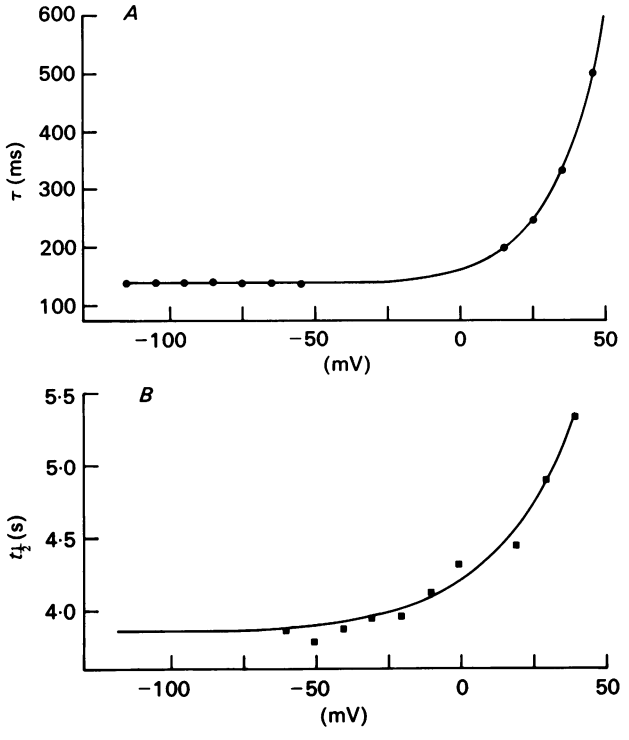

Fig. 19. Effect of voltage on time constant of slow relaxation of current (*A*) and on duration of flash response (*B*). A, points show values of time constant $\tau = 1/\alpha$ used in eqn. (7) to fit the slow change in current after a voltage step from −35 mV in the dark. Same rod as in Fig. 10*B*. *B*, points are the time after a saturating flash at which the light-sensitive current recovered to half its dark level. Same rod as in Fig. 5. Smooth curves in *A* and *B* are exponentials with e-fold changes in 16·8 and 27·8 mV respectively. Resting potential in *B* −31 mV; flash photon density 260 μm^{-2}.

a carrier that required loading with two cations before translocation. If the ions do move in pairs and bind to sites of equal affinity, the inward current at large negative potentials should vary with the square of the external [Na]. This prediction has not been tested under voltage clamp, but with very rapid changes of the ions around the outer segment there is no evidence of a square-law dependence on Na (Hodgkin *et al.* 1985).

An alternative kind of explanation of the rectification would be that it depends on gating or block of the channel by a doubly charged particle. If this were so, the current–voltage relation might relax to the steeply rectifying form during the resolution time of the measurements (roughly 10 ms). Behaviour that is qualitatively like this has been reported for the light-sensitive conductance of barnacle photoreceptors (Brown, Hagiwara, Koike & Meech, 1970), where the current–voltage relation is initially linear but becomes outwardly rectifying in roughly 15 ms. There is evidence of a gating process in rods that operates faster than the resolution time of our measurements: one component of the light-sensitive current noise shows a relaxation time constant of the order of 1 ms (Attwell & Gray, 1984; Bodoia &

Detwiler, 1984; Gray & Attwell, 1985). Nevertheless, if the channel has only two conducting states, open and closed, it seems unlikely that a voltage-dependent gating process can completely account for the rectification that we have observed. Suppose, for example, that the current through an open channel is proportional to the driving force ($V - V_r$) and that the fraction of channels in the open state, f_o, is gated according to

$$f_o = \frac{1}{1 + e^{-(V-V')/S'}}, \tag{11}$$

where V' is the voltage at which $f_o = 0{\cdot}5$ and S' is an exponential steepness parameter. Eqn. (11) applies for a simple voltage-dependent gating or block of the channel by a charged particle. This model predicts that the channels should close completely at large negative potentials and that there should be a region of negative slope resistance at negative voltages. In trying to fit such a model to curve (1) in Fig. 6 it was found that steep outward rectification was inevitably associated with a region of negative resistance at negative voltage. No negative resistance region was observed experimentally. This argument does not exclude the possibility that the open channel has multiple conductance states, as it might if different species of ions (e.g. Ca and Na) required widely different times to pass through. Further tests of the barrier model will require voltage-clamp experiments with better time resolution.

Gating of the channel by voltage and light

A voltage step caused a slow relaxation in the fraction of light-sensitive channels in the conducting state. Although voltage might gate the light-sensitive channel directly, the kinetics seem more consistent with an indirect mechanism in which voltage modulates the concentration of an internal transmitter that gates the channels chemically. Thus the voltage-dependent gating occurred on a time scale comparable to that of the flash response, and the kinetics of gating and flash responses accelerated to a similar degree in background light.

If voltage acts on the channel indirectly, what senses the voltage? A likely candidate is the electrogenic Na/Ca exchanger thought to be present in the surface membrane (Yau & Nakatani, 1984*b*; see also Gold & Korenbrot, 1980, and Yoshikami, George & Hagins, 1980). Hyperpolarization is expected to speed the exchanger and lower the concentration of internal Ca, while depolarization should slow the exchange and raise internal Ca. Several lines of evidence show that a rise in internal Ca leads to closure of light-sensitive channels (e.g. Brown, Coles & Pinto, 1977; Hagins & Yoshikami, 1977; Hodgkin *et al.* 1985). The exchanger is thought to transport three Na for each Ca (Yau & Nakatani, 1984*b*), which would give the rate constant for Ca extrusion a voltage dependence of e-fold in 25 mV. This is like that of the voltage-dependent gating in the simply behaving cells whose steady-state activation declined monotonically with increasing depolarization.

Assuming that the gating does depend on changes in internal Ca, several features remain unexplained. One puzzling feature is the rise in the steady-state activation at positive voltages in the better cells. A possible explanation is that this reflects differences in the voltage dependence of Ca entry through the light-sensitive channels and Ca extrusion by the exchange. Another unexplained feature of the activation curve is that hyperpolarizing the rod below the dark potential could only

increase the fraction of channels open by about a factor of two. In contrast, injections of cyclic GMP (MacLeish *et al.* 1984; Cobbs & Pugh, 1985) or Ca buffers (Matthews, Torre & Lamb, 1985) increase the light-sensitive current by up to a factor of 20. Perhaps the limit on activation of the current by voltage results from increasing Ca entry during hyperpolarization, or from a limit on the rate of Na–Ca exchange.

The S-shaped delay in the response to a voltage step would be expected if internal Ca changed along an exponential time course and affected the light-sensitive conductance in an indirect manner involving another substance. Furthermore, if Ca acted directly on the light-sensitive channel it is difficult to see how background light would speed the relaxation unless the rate constant for Ca extrusion were itself light-sensitive. The observations might be explained by assuming that cyclic GMP acts to keep channels open (Fesenko, Kolesnikov & Lyubarsky, 1985) and that a rise in internal [Ca] lowers the concentration of cyclic GMP by inhibiting the guanylate cyclase (Hodgkin *et al.* 1985). The rate constant for hydrolysis of cyclic GMP might then appear as an additional light-dependent delay in the response to a voltage step.

The slowing of the relaxation observed at positive potentials can be explained by a decrease in the rate of Ca extrusion by the exchange carrier. The concomitant slowing of the flash response and the increase in the relative flash sensitivity probably also result from slowing of the exchange carrier, since similar changes occur when internal [Ca] is raised by lowering external [Na] (e.g. Yau *et al.* 1981; Hodgkin *et al.* 1984).

Correlation between relaxation kinetics and the continuous current noise

Brief voltage noise events in a rod would be expected to result in current noise events having the form of eqn. (9). Indeed, the continuous component of the dark noise described by Baylor *et al.* (1980) was consistent with a superposition of shot events having the form of eqn. (9). Because the variance of this component varied linearly with the length of outer segment in the recording pipette, however, the noise appeared to arise from conductance fluctuations rather than a voltage-driven mechanism. Further studies of the noise under current and voltage clamp should clarify the relative importance of voltage-driven current noise generation at the outer segment. A different connexion between the voltage-dependent gating and the continuous noise might be found if, for example, the noise results from local fluctuations in $[Ca]_i$. In this case the relaxation measurements may reflect the time constants of the noise process which should be briefer in light and slower at positive potentials.

We wish to thank Professor A. L. Hodgkin for helpful suggestions, Dr David Corey and Professors J. E. Brown and W. K. Chandler for advice about voltage-clamp circuitry, and Drs Trevor Lamb, Peter McNaughton and Vincent Torre for comments on the manuscript. Supported by grant EY01543 from the National Eye Institute, USPHS.

REFERENCES

ATTWELL, D. & GRAY, P. (1984). Patch-clamp recordings from rods of the salamander retina. *Journal of Physiology* **351**, 9*P*.

ATTWELL, D. & WILSON, M. (1980). Behaviour of the rod network in the tiger salamander retina mediated by membrane properties of individual rods. *Journal of Physiology* **309**, 287–315.

BADER, C. R., MACLEISH, P. R. & SCHWARTZ, E. A. (1979). A voltage-clamp study of the light response in solitary rods of the tiger salamander. *Journal of Physiology* **296**, 1–26.

BASTIAN, B. L. & FAIN, G. L. (1982). The effects of low calcium and background light on the sensitivity of toad rods. *Journal of Physiology* **330**, 307–329.

BAYLOR, D. A., HODGKIN, A. L. & LAMB, T. D. (1974). The electrical response of turtle cones to flashes and steps of light. *Journal of Physiology* **242**, 685–727.

BAYLOR, D. A. & LAMB, T. D. (1982). Local effects of bleaching in retinal rods of the toad. *Journal of Physiology* **328**, 49–71.

BAYLOR, D. A., LAMB, T. D. & YAU, K.-W. (1979). The membrane current of single rod outer segments. *Journal of Physiology* **288**, 589–611.

BAYLOR, D. A., MATTHEWS, G. & NUNN, B. J. (1984). Location and function of voltage-sensitive conductances in retinal rods of the salamander, *Ambystoma tigrinum*. *Journal of Physiology* **354**, 203–223.

BAYLOR, D. A., MATTHEWS, G. & YAU, K.-W. (1980). Two components of electrical dark noise in retinal rod outer segments. *Journal of Physiology* **309**, 591–621.

BODOIA, R. D. & DETWILER, P. B. (1984). Patch clamp study of the light response of isolated frog retinal rods. *Biophysical Journal* **45**, 337a.

BROWN, H. M., HAGIWARA, S., KOIKE, H. & MEECH, R. M. (1970). Membrane properties of a barnacle photoreceptor examined by the voltage clamp technique. *Journal of Physiology* **208**, 385–413.

BROWN, J. E. & PINTO, L. H. (1974). Ionic mechanism for the photoreceptor potential of the retina of *Bufo marinus*. *Journal of Physiology* **236**, 575–591.

BROWN, J. E., COLES, J. A. & PINTO, L. H. (1977). Effects of injections of calcium and EGTA into the outer segments of retinal rods of *Bufo marinus*. *Journal of Physiology* **269**, 707–722.

BROWN, P. K., GIBBONS, R. I. & WALD, G. (1963). The visual cells and visual pigments of the mudpuppy, *Necturus*. *Journal of Cell Biology* **19**, 76–106.

CAPOVILLA, M., CARETTA, A., CERVETTO, L. & TORRE, V. (1983). Ionic movements through light-sensitive channels of toad rods. *Journal of Physiology* **343**, 295–310.

COBBS, W. H. & PUGH, E. N. (1985). Cyclic GMP can increase rod outer segment light-sensitive current 10-fold without delay of excitation. *Nature* **313**, 585–587.

DETWILER, P. B., HODGKIN, A. L. & MCNAUGHTON, P. A. (1978). A surprising property of electrical spread in the network of rods in the turtle's retina. *Nature* **274**, 562–565.

DETWILER, P. B., HODGKIN, A. L. & MCNAUGHTON, P. A. (1980). Temporal and spatial characteristics of the voltage response of rods in the retina of the snapping turtle. *Journal of Physiology* **300**, 213–250.

FESENKO, E. E., KOLESNIKOV, S. S. & LYUBARKSY, A. L. (1985). Induction by cyclic GMP of cationic conductance in plasma membrane of retinal rod outer segment. *Nature* **313**, 310–313.

FUORTES, M. G. F. & HODGKIN, A. L. (1964). Changes in time scale and sensitivity in the ommatidia of Limulus. *Journal of Physiology* **172**, 239–263.

GOLD, G. H. (1979). Photoreceptor coupling in the retina of the toad *Bufo marinus*. II. Physiology. *Journal of Neurophysiology* **42**, 311–328.

GOLD, G. H. (1981). Photoreceptor coupling: its mechanism and consequences. In *Current Topics in Membranes and Transport. vol. 15, Molecular Mechanisms of Photoreceptor Transduction*. ed. MILLER, W. H., pp. 59–89. New York: Academic Press.

GOLD, G. H. & KORENBROT, J. I. (1980). Light-induced Ca release by intact retinal rods. *Proceedings of the National Academy of Sciences of the United States of America* **77**, 5557–5561.

GRAY, P. & ATTWELL, D. (1985). Kinetics of light-sensitive channels in vertebrate photoreceptors. *Proceedings of the Royal Society* B, **223**, 379–388.

HAGINS, W. A., PENN, R. D. & YOSHIKAMI, S. (1970). Dark current and photocurrent in retinal rods. *Biophysical Journal* **10**, 380–412.

HAGINS, W. A. & YOSHIKAMI, S. (1977). Intracellular transmission of visual excitation in photoreceptors: electrical effects of chelating agents introduced into rods by vesicle fusion. In *Vertebrate Photoreception*, ed. BARLOW, H. B. & FATT, P., pp. 97–139. London: Academic Press.

HODGKIN, A. L. & KEYNES, R. D. (1955). The potassium permeability of a giant nerve fibre. *Journal of Physiology* **128**, 61–88.

HODGKIN, A. L., MCNAUGHTON, P. A., NUNN, B. J. & YAU, K.-W. (1984). Effect of ions on retinal rods from *Bufo marinus*. *Journal of Physiology* **350**, 649–680.

HODGKIN, A. L., MCNAUGHTON, P. A. & NUNN, B. J. (1985). The ionic selectivity and calcium dependence of the light-sensitive pathway in toad rods. *Journal of Physiology* **358**, 447–468.

JACK, J. J. B., NOBLE, D. & TSIEN, R. W. (1975). *Electric Current Flow in Excitable Cells*. Oxford: Clarendon Press.

LAMB, T. D., MCNAUGHTON, P. A. & YAU, K.-W. (1981). Spatial spread of activation and background desensitization in toad rod outer segments. *Journal of Physiology* **319**, 463–496.

MACLEISH, P. R., SCHWARTZ, E. A. & TACHIBANA, M. (1984). Control of the generator current in solitary rods of the *Ambystoma tigrinum* retina. *Journal of Physiology* **348**, 645–664.

MATTHEWS, H. R., TORRE, V. & LAMB, T. D. (1985). Effects on the photoresponse of calcium buffers and cyclic GMP incorporated into the cytoplasm of retinal rods. *Nature* **313**, 582–585.

NACE, G. W. (1974). *Amphibians. Guidelines for the breeding, care and management of laboratory animals*. Washington, D.C.: National Academy of Sciences.

SCHWARTZ, E. A. (1973). Responses of single rods in the retina of the turtle. *Journal of Physiology* **232**, 503–514.

SCHWARTZ, E. A. (1976). Electrical properties of the rod syncytium in the retina of the turtle. *Journal of Physiology* **257**, 379–406.

YAU, K.-W., MCNAUGHTON, P. A. & HODGKIN, A. L. (1981). Effect of ions on the light-sensitive current of retinal rods. *Nature* **292**, 502–505.

YAU, K.-W. & NAKATANI, K. (1984*a*). Cation selectivity of light-sensitive conductance in retinal rods. *Nature* **309**, 352–354.

YAU, K.-W. & NAKATANI, K. (1984*b*). Electrogenic Na–Ca exchange in retinal rod outer segment. *Nature* **311**, 661–663.

YOSHIKAMI, S., GEORGE, J. S. & HAGINS, W. A. (1980). Light-induced Ca fluxes from outer segment layer of vertebrate retinas. *Nature* **286**, 395–398.